Polarimetric Signatures from the Base of Icebergs in BIOMASS P-band SAR Images

Georg Fischer, Jun-Su Kim, Irena Hajnsek and Konstantinos P. Papathanassiou

***Abstract*—The polarimetric signatures of tabular icebergs floating off the coast of Antarctica were among the most distinctive ones observed by ESA's BIOMASS mission during its in-orbit commissioning phase. In addition to the polarimetric response of the iceberg itself, a time-delayed replica appears as the result of scattering interactions at the icebergs' base. Polarimetric analyses and a simple geometric model are used to investigate the scattering mechanisms at the top and base of icebergs as well as their relative range displacement. The relationship between range displacements and thickness indicates a potential penetration depth of the P-band signal in firn and ice of up to 250–300 m.**

***Index Terms*— Synthetic Aperture Radar, Polarimetry, Antarctica, Penetration Depth, Iceberg Thickness**

I. Introduction

ESA's BIOMASS mission, launched in April 2025, operates a fully polarimetric P-band Synthetic Aperture Radar (SAR) at a frequency of 435 MHz (wavelength $\lambda \approx 69$ cm) [1]. The long wavelength enables penetration into dry snow, firn, and ice, which allows unique subsurface mapping applications on glaciers, ice sheets, and icebergs [2].

During the commissioning phase of the mission, one of the most noticeable observations was the polarimetric signature of tabular icebergs floating off the coast of Antarctica. Besides the primary polarimetric response of the iceberg itself, a time-delayed replica with a distinct and often different polarimetric signature appears for most of the analyzed examples. These replicas have been hypothesized to be the result of scattering interactions occurring at the base of the icebergs.

While the detection of icebergs in (polarimetric) SAR data is widely studied [3], there are only very rare cases, where contributions from the base of icebergs were observed. In a pioneering contribution [4], time-delayed replicas of Arctic icebergs in airborne L-band data in HH and HV polarizations were reported. The authors interpreted these replicas as (time-delayed) reflections from ice-water interface facets at the base and the walls of the irregularly shaped icebergs. They concluded a specular reflection, either from normal local incidence or dihedrals, as the ice-water scattering mechanism. The extent of the replicas was smaller than the direct iceberg return and measured distances related to reasonable iceberg thicknesses of e.g. about 35 m.

The question is how far these results transfer to the case of the iceberg replicas in the BIOMASS acquisitions. Antarctic tabular icebergs have sizes of up to several kilometers and few hundreds of meters thickness. Furthermore, they calve of ice shelves with firn bodies that experience seasonal melt, causing refrozen melt layers and inclusions (ice lenses and pipes), which are known to cause strong scattering in the first tens of meters of firn below the surface [5],[6].

The aim of this letter is to provide a physical interpretation of the polarimetric signature of tabular icebergs in BIOMASS data and to introduce a first-order understanding of the scattering mechanisms occurring at the top and the base of the icebergs. Further, the range displacement between the top and base contributions is related to iceberg thickness and allows insights into the penetration depth of P-band signals in firn and ice.

II. Polarimetric Descriptors & Scattering Processes

The polarimetric analysis is based on the full polarimetric Pauli scattering vector. The first Pauli channel, HH+VV, is high for surface scattering, the second, HH-VV, for dihedral scattering and the third, HV+VH, for volume scattering [7]. The polarimetric scattering entropy H and scattering alpha angle α are derived from the polarimetric covariance matrix [7]. Entropy $0 \leq H \leq 1$ indicates the polarimetric complexity (i.e. dimensionality) of the scattering process. The scattering alpha angle $0° \leq \alpha \leq 90°$ indicates the type of scattering, ranging from surface scattering (low α, bluish colors in **Fig. 1** and **Fig. 2**) to dipole or volume scattering (medium α) and dihedral scattering (high α, reddish colors in **Fig. 1** and **Fig. 2**).

Tabular icebergs have a more or less rectangular profile, with a flat top, steep sides, and a relatively flat base. Even though this profile degrades over time [8],[9], it can be used to address the polarimetric signature of such icebergs. The penetration of the P-band signal allows contributions from the top as well as the base, i.e. the ice-water interface. The top scattering contributions likely originate not only from the actual surface, but also from layers in the first tens of meters below the iceberg surface [6]. Different scattering mechanisms are possible:

- Surface scattering, characterised by low entropy and low alpha is interpretated as originating from horizontal layers. As their roughness increases, so do H and α values, while the transmission into the ice volume decreases.

Georg Fischer, Jun-Su Kim, Irena Hajnsek, and Konstantinos P. Papathanassiou are with the Microwaves and Radar Institute (HR) of the German Aerospace Center (DLR). Irena Hajnsek is also with the Institute of Environmental Engineering of ETH Zurich.

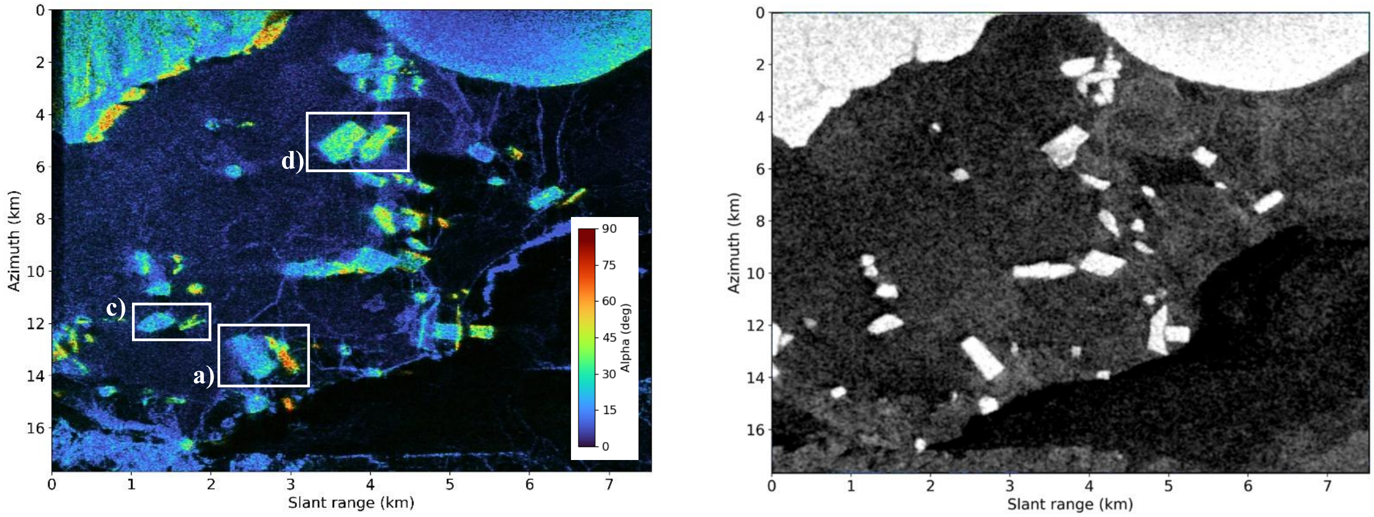

Fig. 1. Left: Hue-Saturation-Intensity (HSI) polarimetric BIOMASS image in radar coordinates of icebergs in front of the Jelbart ice shelf (at top left) in Antarctica (70.4°S, 5.8°W). Hue = polarimetric α angle, Saturation = 1, Intensity = total backscatter. The tops of icebergs mostly appear blue, indicating surface scattering contributions, paired by a time-delayed, often dihedral, scattering contribution, as indicated by the reddish colors, from the base of the iceberg. The white boxes indicate the icebergs analyzed in Section V. **Right:** Sentinel-1 HH backscatter image acquired one day earlier where no scattering replicas are visible.

- Volume scattering, with a medium/high H and medium α, is known to result from ice inclusions (ice lenses and pipes) [5].

Also, at the base of the iceberg, different scattering mechanisms are possible:

- Direct, surface scattering from the ice-water interface (light blue in **Fig. 3**), only affected by refraction at the air-ice transition. Such a base surface scattering is characterised by low H and low α values that increase with increasing roughness of the ice-water interface.
- Dihedral scattering between the base reflection and scatterers at or near the top (orange in **Fig. 3**). The latter could be either forward scattering through the (rough) top surface or reflection at ice inclusions. Both processes are characterised by high α and low to medium H.

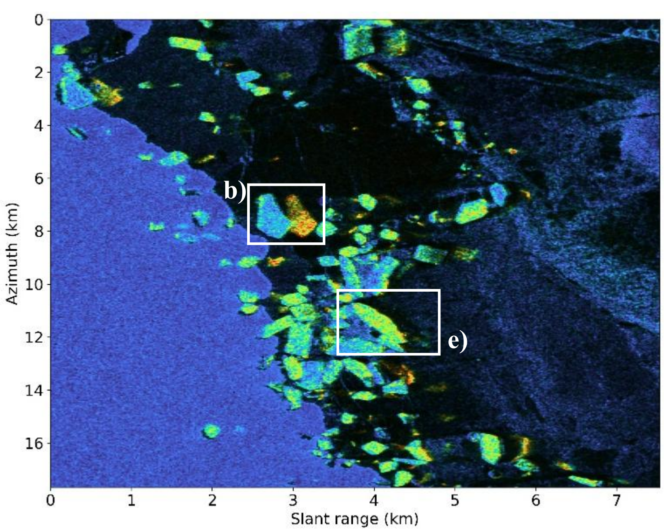

Fig. 2. BIOMASS HSI image of icebergs with strong extended dihedral base signature and without base signature (66.2°S, 85.3°E). White boxes show examples analyzed in Section V.

In the presence of both mechanisms at the base, α reaches intermediate values while H levels increase. It is important to note here that the dihedral scattering occurring at the base of the iceberg generates a spatially extended dihedral signature. This is different to localized dihedral signatures generated by interactions between the base and back wall or between the water and the front wall. In the following, these mechanisms, alone or superimposed to each other, will be used to interpret the observed polarimetric signature of icebergs in the BIOMASS data.

TABLE I
DATASETS USED

Dataset	Shown in	Identifier
BIOMASS	Fig. 1	20250623T072557_20250623T072726
BIOMASS	Fig. 2	20251104T113434_20251104T113549
Sentinel-1C	Fig. 1	EW 20250622T204748_20250622T204853

III. Icebergs In BIOMASS Data

The used BIOMASS data, listed in Table I, were acquired during the commissioning phase of the mission. The data sets have been processed by ESA's Ground Processor Prototype (GPP) that performs SAR focusing, geolocation, polarimetric calibration as well as ionospheric (including Faraday rotation) correction [10]. The time delay between the iceberg top and base manifests as a range displacement between iceberg and replica as seen in **Fig. 1** and **Fig. 2**.

Following polarimetric patterns can be observed:

i) Icebergs with a surface-scattering like top contribution, characterised by low H and low α values (bluish colours in **Fig. 1** and **Fig. 2**) are paired with replicas characterised by strong extended dihedral contributions with high α values (reddish colours in **Fig. 1** and **Fig. 2**).

ii) Icebergs with a similar surface-scattering like top contribution (low H, low α) can have a replica with medium H

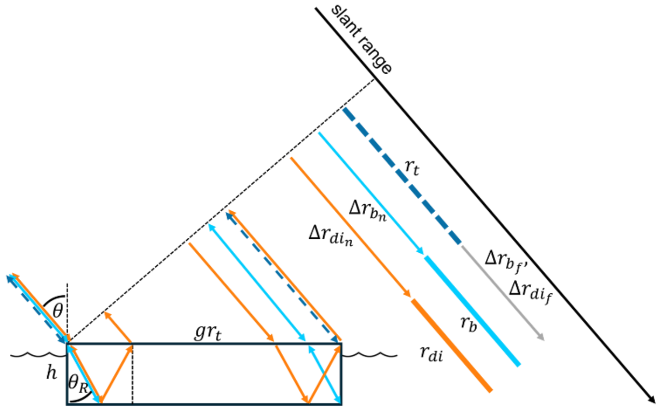

Fig. 3. Rectangular profile of an iceberg with ground-range size gr_t and thickness h and its projection into slant range. First and last possible signal paths as well as range lengths r_x and displacements Δr_x are indicated for the top signal (dark blue, dashed), direct base (light blue) and dihedral base (orange).

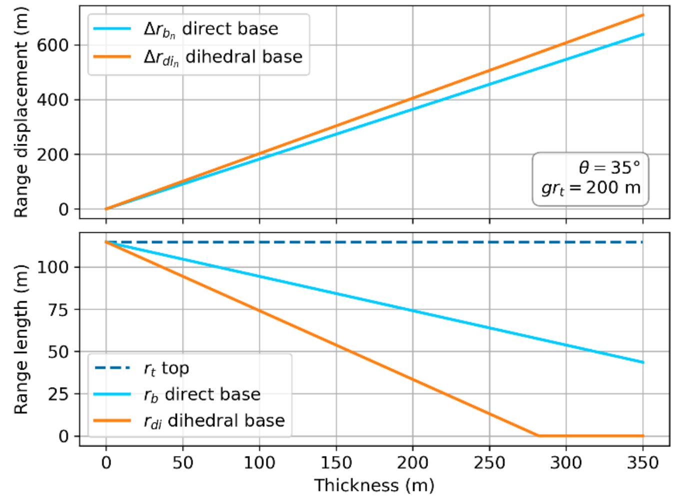

Fig. 4. Top: Range displacements between the near range edge of the top and base signal, assuming a direct and dihedral base scattering. **Bottom**: Range lengths of the top, direct base, and dihedral base contributions. Simulated iceberg with 200 m ground range size, thickness 0 – 350 m, at 35° incidence angle.

and medium α. This can be the result of the superposition of two base contributions: direct, surface scattering from the ice-water interface, and dihedral scattering.
iii) Icebergs with a top contribution characterised by medium H and medium α (greenish colours in **Fig. 1** and **Fig. 2**), can have replicas with a similar (e.g., medium H, medium α) behaviour.
iv) The icebergs which do not have a replica are characterised by a top signature of high H and medium α.

The geometry of these scattering processes and their range displacements relative to each other is discussed next.

IV. Geometry of Scattering Mechanisms

Based on the rectangular profile of tabular icebergs, a first-order geometry model is introduced, see **Fig. 3**. Accordingly, the range displacement between iceberg and replica, as well as the length (i.e., extent) of the replica, depend on the thickness and the size (i.e., range extent) of the iceberg. The slant-range length $r_t = gr_t \sin\theta$ of the icebergs' top is related to the ground-range length gr_t via incidence angle θ.

The slant-range extent of the base contribution is shorter than the extent of the top contribution, and depends on the iceberg thickness h. It is different for the direct r_b and the dihedral contributions r_{di} (the latter is shorter)

$$\begin{aligned} r_b &= r_t - h\tan\theta_R \sin\theta, \\ r_{di} &= r_t - 2h\tan\theta_R\sin\theta, \end{aligned} \tag{1}$$

where θ_R is the refracted incidence angle. The displacement of the near-range edge of the top and base contribution differs for a direct Δr_{b_n} and dihedral scattering Δr_{di_n}

$$\begin{aligned} \Delta r_{b_n} &= \frac{h\sqrt{\epsilon}}{\cos\theta_R}, \\ \Delta r_{di_n} &= h\left(\frac{\sqrt{\epsilon}}{\cos\theta_R} + \tan\theta_R \sin\theta\right). \end{aligned} \tag{2}$$

A bulk permittivity ϵ of 2.95 [11],[12] is assumed for calculating θ_R and the range displacements. The corresponding bulk density is 850 kg/m³ indicating the iceberg's freeboard to be 17% of its thickness.

The far-range displacement of the top and base contributions Δr_{b_f} , Δr_{di_f} is equal for both direct and dihedral scattering, since the phase center of the last possible base contribution is located at the base-back wall corner for both

$$\Delta r_{b_f} = \Delta r_{di_f} = h\left(\frac{\sqrt{\epsilon}}{\cos\theta_R} - \tan\theta_R \sin\theta\right). \tag{3}$$

Note that the replica can be the superposition of both base contributions, direct surface scattering and dihedral. How strong these are relative to each other, and relative to the top contribution, depends widely on the air-ice (top) and ice-water (base) interfaces. Smooth top air-ice interfaces increase the transmission into the iceberg volume, increasing the base contributions (replicas) while weakening the top contribution. Rough ice-water interfaces increase the direct surface and attenuate the dihedral base component.

Range displacements and range lengths for direct and dihedral base contributions are simulated as function of thickness for an iceberg with a 200 m ground range size in **Fig. 4**. The differences in range displacements between the direct and dihedral base contributions are small for an incidence angle of $\theta = 35°$, which is a large value for BIOMASS acquisition geometries. The difference decreases further for steeper incidence angles. The influence of thickness on the range lengths also decreases at steeper incidence angles and is about one order of magnitude smaller than on range displacements. For thicknesses larger than the ground-range size, dihedral scattering becomes impossible, as large parts of the icebergs base are in the "shadow" of the water.

Other reasons for a missing base contribution include increased attenuation from seasonal melting, increased scattering losses, e.g., from volume scattering at ice inclusions inside the firn, or a too large thickness for P-band penetration.

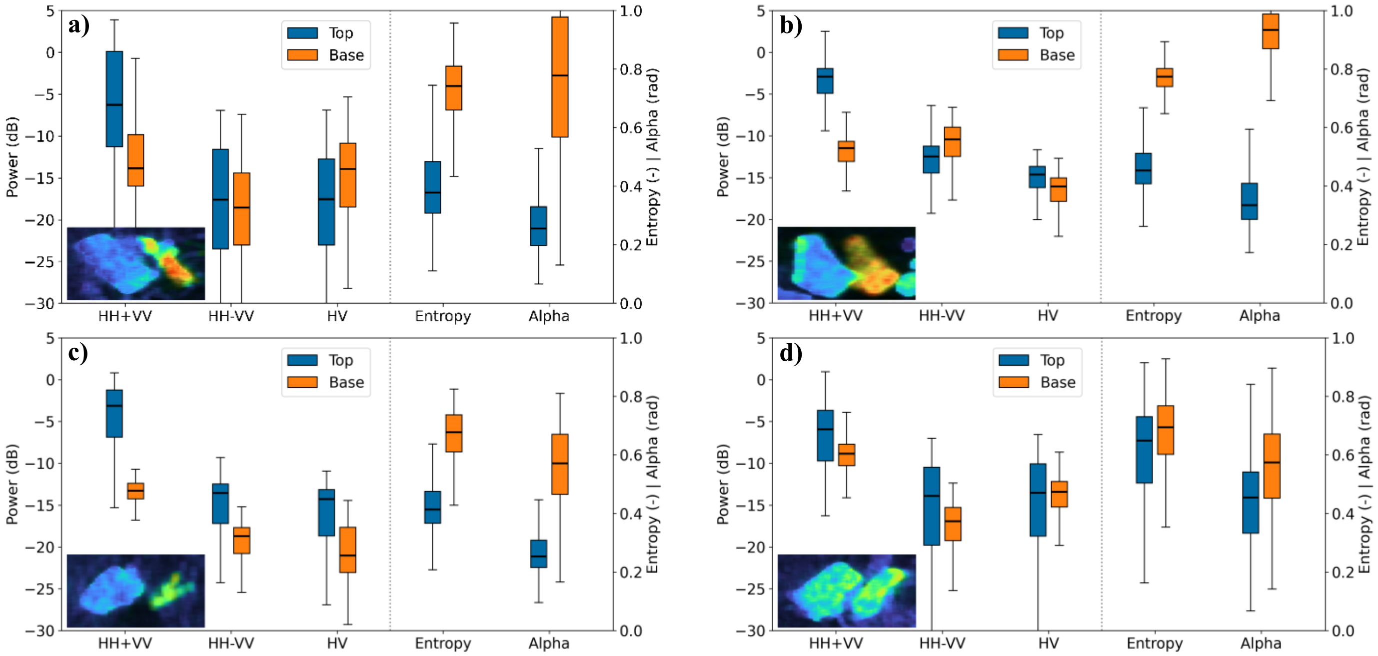

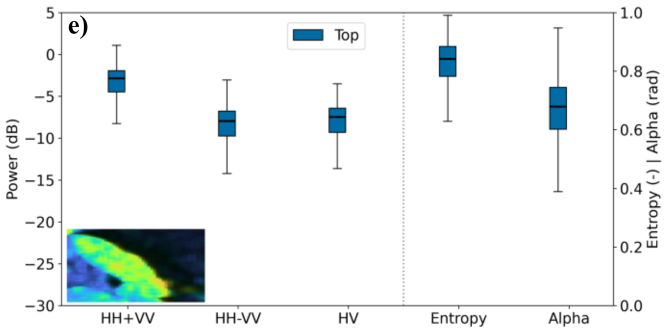

Fig. 5. Statistics of backscatter values of Pauli channels and polarimetric entropy H and alpha α for top and base signals. The colored boxes extend from first to third quartile, with the black line at the median. Whiskers extend to the farthest data point within 1.5x box size. Examples **a)** – **e)** are indicated with white boxes in **Fig. 1** and **Fig. 2**.

V. Polarimetric Analysis of Scattering Mechanisms

The previous section makes it clear that the geometry alone is not sufficient to characterize the scattering processes. For this, backscattered powers and polarimetric parameters from top and base contributions of representative examples are evaluated and discussed. For this, **Fig. 5** shows the backscattered powers for the three Pauli channels as well as entropy and alpha values of the top and base contribution for five different iceberg cases. The colored boxes indicate the first to third quartile, with a black line as median. The values are extracted with an 18 x 3 (azimuth x range) multi-looking.

The cases in **Fig. 5a** and **b** fit the initial observation with a surface scattering mechanism at the top of the iceberg, with high HH+VV and low entropy and alpha. The base dihedral has a median alpha of 44.5° and 53.5°, respectively, which is among the highest observed. Interestingly, HH-VV and HV is similar or even higher for the base compared to the top. This points to an efficient dihedral mechanism, considering the top backscatter acts as scattering losses for the base contribution, with further losses at reflection and propagation. The second interaction of such a mechanism could be forward scattering through the (rough) top surface or a reflection at ice inclusions inside the firn. However, such inclusions would also produce strong volume scattering from the top [5], which is not observed in these cases.

The case in **Fig. 5c** has similar low-alpha surface scattering from the top. The base contribution shows weaker HH-VV and HV backscatter as well as lower alpha compared to **Fig. 5a** and **b**. This could be interpretated as a superposition of direct and dihedral base contributions.

Fig. 5d is an example for a top and base signature of medium H and medium α with similar values for all parameters. The reason could be that volume scatterers near the surface (ice inclusions in firn) influence both the top contribution and the base dihedral.

For icebergs with strong volume scattering at the top (high H, medium α, high backscatter in all polarizations), the base contribution may disappear, see **Fig. 5e**. This indicates strong scattering losses preventing signal penetration down to the base.

The data analysis reveals a widely consistent pattern: Those icebergs with surface scattering at the top have the most distinct dihedral base contribution.

VI. The Relationship to Thickness

Assuming a direct or dihedral base scattering mechanism and an ideal rectangular iceberg profile provides a direct link to thickness, as already suggested in [4], by inverting (2) and (3). Measured range displacements between top and base

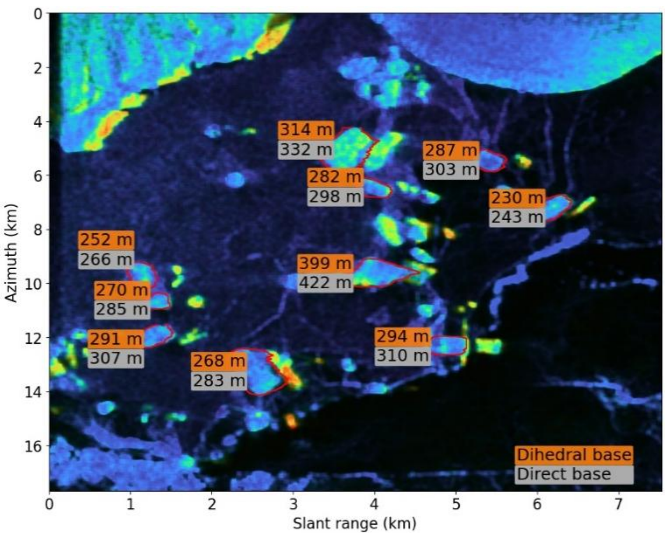

Fig. 6. Thickness of icebergs estimated by inverting eq. (2) based on range displacements measured at the near range edge of the iceberg top and base signatures. Assuming a dihedral (orange) or direct (grey) base scattering mechanism.

contributions result in thicknesses between 250 m and 300 m for the iceberg examples in **Fig. 6**. Values above 300 m are clearly related to inaccurate iceberg top and base delineations. The difference between assuming a direct or dihedral base mechanism is roughly 20 m for measurements of near range edge displacements (**Fig. 6**), in accordance with **Fig. 4 top**.

Further, there is a systematic difference in thickness between near and far range edge measurements. Far range displacements always result in smaller thicknesses, by 10 m to 60 m. Two possible reasons are: First, the shape of tabular icebergs changes over time due to wave erosion and melt, developing a “foot” protruding under water with rounded-off edges [8], [9]. Second, the top signal is not (only) from the actual surface, but from the first few tens of meters of firn [6]. Thus, the last possible top contribution at the far range edge can originate from deeper layers. Both phenomena lead to an effectively smaller thickness at the far range edge.

Note that iceberg shape deviations from the simple geometry model affect the thickness estimates. Densities at the coast of Antarctica [11] and of individual icebergs [12] translate into bulk permittivities of 2.8 – 3.0, leading to a thickness uncertainty of 4%. An uncertainty of one BIOMASS range resolution cell of 25 m propagates into a thickness uncertainty of about 18 m for the difference of two range measurements. This can be reduced to, e.g., about 6 m by averaging 10 measurements at independent azimuth positions. No coinciding validation data was found, but ICESat-2 data from 15 days earlier in the area of **Fig. 6** indicate icebergs with a freeboard of ~40 m [13], corresponding to ~235 m thickness.

VII. Conclusions

Time-delayed contributions from the base of icebergs provide clear evidence that BIOMASS P-band signals can penetrate 250-300 m into snow, firn, and ice in the analyzed examples. This is deeper than reported from airborne SAR experiments over areas with refrozen melt inclusions in the near-surface firn. The reason is the strong reflection at the ice-water interface that enables the detection of a scattering contribution from the base of icebergs. The proposed understanding of scattering contributions occurring at the top and the base of the icebergs allows the interpretation of their polarimetric signatures and their relative range displacements. The unique signature of an extended dihedral scattering mechanism is interpretated as an interaction between a reflection at the base ice-water interface and either forward scattering through a rough surface at the top or reflections at ice inclusions inside the firn. Assuming a simplified iceberg geometry, the link of the range displacement between the top and base contributions to the iceberg thickness is provided. Towards a thickness application, the challenge is the detection and accurate delineation of the iceberg top and base signatures. The strong backscatter of up to -10 dB from down to 300 m deep base contributions suggests that the detection of significantly deeper scatterers is possible.

References

[1] S. Quegan et al., “The European space agency BIOMASS mission: Measuring forest above-ground biomass from space,” Remote Sens. Environ., vol. 227, pp. 44–60, Jun. 2019.

[2] K. Scipal et al., “BIOMASS: ESA’s P-Band SAR Mission,” Proc. IEEE, pp. 1–16, 2026, doi: 10.1109/JPROC.2026.3687416.

[3] W. Dierking and C. Wesche, “C-Band Radar Polarimetry—Useful for Detection of Icebergs in Sea Ice?,” IEEE Trans. Geosci. Remote Sensing, vol. 52, no. 1, pp. 25–37, Jan. 2014, doi: 10.1109/TGRS.2012.2234756.

[4] A. L. Gray and L. D. Arsenault, “Time-delayed reflections in L-band synthetic aperture radar imagery of icebergs,” IEEE Trans. Geosci. Remote Sensing, vol. 29, no. 2, pp. 284–291, Mar. 1991, doi: 10.1109/36.73670.

[5] E. Rignot, “Backscatter model for the unusual radar properties of the Greenland Ice Sheet,” Journal of Geophysical Research, vol. 100, no. E5, Art. no. E5, 1995, doi: 10.1029/95JE00485.

[6] G. Fischer, M. Jäger, K. P. Papathanassiou, and I. Hajnsek, “Modeling the Vertical Backscattering Distribution in the Percolation Zone of the Greenland Ice Sheet With SAR Tomography,” IEEE J. Sel. Top. Appl. Earth Obs. Remote Sens., vol. 12, no. 11, Art. no. 11, Nov. 2019, doi: 10.1109/JSTARS.2019.2951026.

[7] S. Cloude, Polarisation: applications in remote sensing, 1st ed. Oxford ; New York: Oxford University Press, 2010.

[8] M. R. England, T. J. W. Wagner, and I. Eisenman, “Modeling the breakup of tabular icebergs,” Sci. Adv., vol. 6, no. 51, p. eabd1273, Dec. 2020, doi: 10.1126/sciadv.abd1273.

[9] T. J. W. Wagner et al., “The ‘footloose’ mechanism: Iceberg decay from hydrostatic stresses,” Geophysical Research Letters, vol. 41, no. 15, pp. 5522–5529, Aug. 2014, doi: 10.1002/2014GL060832.

[10] J. S. Kim, K. P. Papathanassiou, R. Scheiber, and S. Quegan, “Correcting Distortion of Polarimetric SAR Data Induced by Ionospheric Scintillation,” IEEE Trans. Geosci. Remote Sensing, vol. 53, no. 12, pp. 6319–6335, Dec. 2015, doi: 10.1109/TGRS.2015.2431856.

[11] S. R. M. Ligtenberg, M. M. Helsen, and M. R. van den Broeke, “An improved semi-empirical model for the densification of Antarctic firn,” The Cryosphere, vol. 5, no. 4, Art. no. 4, Oct. 2011, doi: 10.5194/tc-5-809-2011.

[12] A. Braakmann-Folgmann, A. Shepherd, L. Gerrish, J. Izzard, and A. Ridout, “Observing the disintegration of the A68A iceberg from space,” Remote Sens. Environ., vol. 270, p. 112855, Mar. 2022, doi: 10.1016/j.rse.2021.112855.

[13] B. Smith *et al.*, “ATLAS/ICESat-2 L3A Land Ice Height (ATL06, Version 7). [ATL06_20250608072933_12732710_007_01]. NASA NSIDC Distributed Active Archive Center, Boulder, CO, USA, 2025. https://doi.org/10.5067/ATLAS/ATL06.007. Accessed 06-03-2026.